International Journal of Fluid Machinery and Systems
Vol. 9, No. 1, January-March 2016

DOI: 10.5293/IJFMS.2016.9.1.047
ISSN (Online): 1882-9554

Original Paper

Study on Performance Improvement of an Axial Flow Hydraulic Turbine with a Collection Device

Yasuyuki Nishi[1], Terumi Inagaki[2], Yanrong Li[2], Sou Hirama[3] and Norio Kikuchi[4]

[1]Department of Mechanical Engineering, Ibaraki University
4-12-1 Nakanarusawa-cho, Hitachi-shi, Ibaraki, 316-8511, Japan, y-nishi@mx.ibaraki.ac.jp
[2]Department of Mechanical Engineering, Ibaraki University
4-12-1 Nakanarusawa-cho, Hitachi-shi, Ibaraki, 316-8511, Japan
[3]Graduate School of Science and Engineering, Ibaraki University
4-12-1 Nakanarusawa-cho, Hitachi-shi, Ibaraki, 316-8511, Japan
[4]Ibasei, Ltd.
4-7-10 Kamine-cho, Hitachi-shi, Ibaraki, 317-0064, Japan

Abstract

The portable hydraulic turbine we previously developed for open channels comprises an axial flow runner with an appended collection device and a diffuser section. The output power of this hydraulic turbine was improved by catching and accelerating an open-channel water flow using the kinetic energy of the water. This study aimed to further improve the performance of the hydraulic turbine. Using numerical analysis, we examined the performances and flow fields of a single runner and a composite body consisting of the runner and collection device by varying the airfoil and number of blades. Consequently, the maximum values of input power coefficient of the Runner D composite body with two blades (which adopts the MEL031 airfoil and alters the blade angle) are equivalent to those of the composite body with two blades (MEL021 airfoil). We found that the Runner D composite body has the highest turbine efficiency and thus the largest power coefficient. Furthermore, the performance of the Runner D composite body calculated from the numerical analysis was verified experimentally in an open-channel water flow test.

Keywords: Hydraulic Turbine, Runner, Collection Device, Airfoil, Performance, Flow Field

1. Introduction

Among the many alternative natural energy sources available, hydropower has again recently attracted attention for electricity generation because of its high energy density and lower fluctuations compared with other renewable sources. The hydraulic turbines that are used to generate electrical power using waterpower are broadly classified into those for pipe conduits [1] and those for open channels [2-4]. Hydraulic turbines for pipe conduits need to have water stored in a dam or a water tank, from which the water free falls through the pipes and the embodied potential energy is converted into rotational energy of the turbines. However, damming the water may have a negative influence on the ecosystem. Furthermore, suitable locations for installing new such hydropower systems are becoming lesser.

On the other hand, hydraulic turbines for open channels require little infrastructure for guiding the water and can utilize open-channel water flows with low head (small drop in altitude). However, locations for this technology are limited because many of the existing hydraulic turbines for open channels are equipped with intake weirs and tend to have a low rotational speed and need a larger size. Recently, despite the development of hydraulic turbines that can generate power simply by being placed in the path of flow [5-7], the available turbine output power per unit water-receiving area is inadequate.

We have proposed a new type of portable hydraulic turbine that uses the kinetic energy of flow in open channels by applying the principle of a diffuser wind turbine [8] with an attached brim [9, 10]. To improve output power, this hydraulic turbine contains an axial flow runner with an appended collection device that includes a diffuser section to accelerate the water flow. The height of the open-channel-type turbine is restricted by water depth in an open channel. Hence, the diffuser section of the collection device is fixed in the height direction and elongated in the transverse direction. Thereby, the outer diameter of the runner can be mostly enlarged to the same size with the water depth. Moreover, because a high-speed rotation-type runner is adopted, small size and a weight saving can be

Received June 30 2015; accepted for publication August 7 2015: Review conducted by Tadashi Tanuma, Ph.D. (Paper number O15032J)
Corresponding author: Yasuyuki Nishi, y-nishi@mx.ibaraki.ac.jp

attained and it is advantageous also in respect of matching with a generator. Using steady flow analysis, we previously studied the performance and flow field of the open-channel hydraulic turbine with respect to a single runner, a single collection device, and a composite body consisting of the runner and collection device. We also experimentally verified the effectiveness of this hydraulic turbine from analysis results [9, 10]. Furthermore, we clarified the influence of the interference between the runners (with different number of blades) and an axially asymmetrical collection device of the hydraulic turbine [11].

The objective of this study was to improve the performance of an axial flow hydraulic turbine with a collection device. Therefore, through numerical analysis, we investigated the performances and flow fields of a single runner and a composite body consisting of a runner and collection device by varying the airfoil and number of blades. In addition, we conducted an experiment using a real waterway to evaluate and verify the modeling results.

2. Hydraulic Turbine Test Piece

For example, a schematic of the hydraulic turbine test piece for Runner D composite body is shown in Fig. 1, and the coordinate system [9-11] is shown in Fig. 2. The hydraulic turbine uses the principles of the diffuser wind turbine [8] with an attached brim and comprises a collection device (C.D.) appended to an axial flow runner. The hydraulic turbine was designed for a flow velocity v_∞ = 1.5 m/s and open-channel installation in a water depth of 400 mm. The blade phase angle θ* was taken to be positive from the *z*-axis counterclockwise when viewed from the inlet side. When the reference blade is positioned in the positive direction of the *z*-axis (the position in Fig. 4 described below), θ* is defined to be 0°.

The collection device was composed of an inlet nozzle section, a diffuser section, and a brim. Open channels with shallow water depth are constrained in the height direction. Accordingly, the hydraulic turbine described here differs from conventional wind turbines [8, 12-14] and hydraulic turbines [15-18] in which the diffuser section of the collection device is constant vertically and varies horizontally. The brim was attached to the left and right sides of the outlet of the collection device. Thus, it is possible to make the runner outer diameter almost as large as the water depth by making the height of the diffuser section the same as the water depth. The height of the diffuser section was 400 mm to match the design water depth, the spread angle was 8.1° and the length of each brim was 100 mm. The total length of the collection device was 1085 mm.

Figures 3(a)–3(d) illustrate the four runners used for trial in this study, and its dimensions are listed in Table 1. Runner A contained the prototype runner that were designed based on the blade element momentum theory [9, 10]. Three blades were used where the airfoil was consistent with the MEL021 [19] with a maximum blade thickness relative to a chord length. The design value of attack angle was 5°. Runner B was a two-blade runner that was simply designed based on the three blades of Runner A [11]. Runner C was changed into MEL031 [19] which has a low drag-lift ratio for low Reynolds numbers (1×10^5) in the airfoil of Runner B. Runner D was an improved version of runner C, with the blade angle changed. To increase the output power, the outer diameter of each runner was designed to approximately match the designed water depth.

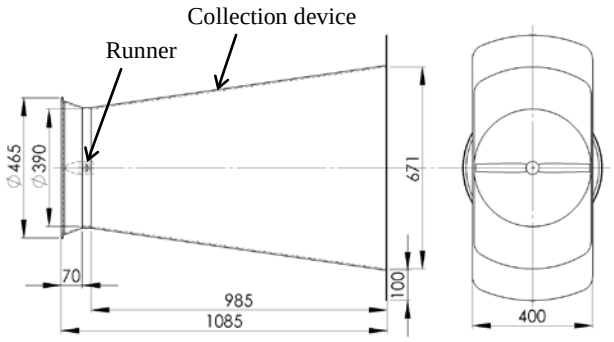

Fig. 1 Hydraulic turbine (Runner D + C.D.)

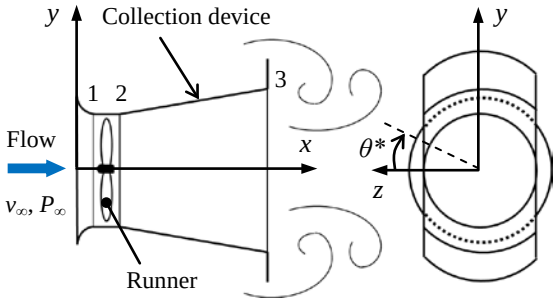

Fig. 2 The definition of a coordinate system

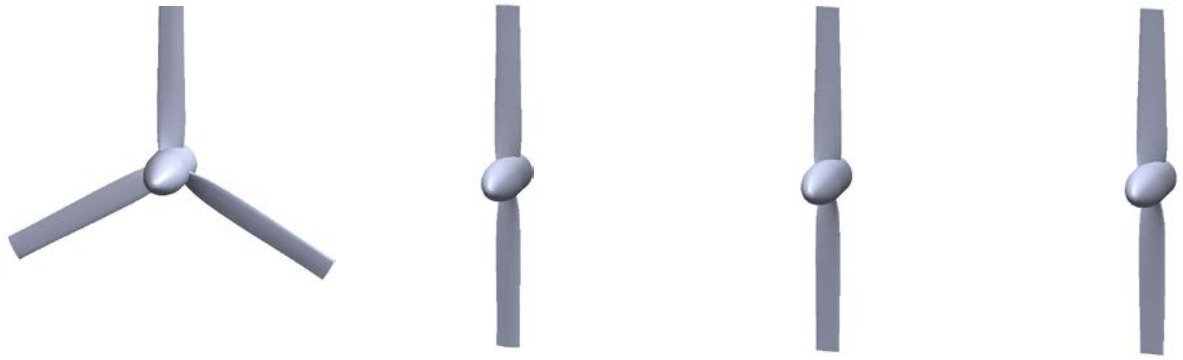

(a) Runner A (b) Runner B (c) Runner C (d) Runner D

Fig. 3 Test runners

Table 1 Specifications of test runners

		Hub	Mid	Tip			Hub	Mid	Tip
Runner A	Radius r [m]	0.019	0.095	0.171	Runner C	Radius r [m]	0.019	0.095	0.171
	Solidity	0.596	0.090	0.025		Solidity	0.397	0.060	0.016
	Blade angle θ [°]	42.95	7.50	2.02		Blade angle θ [°]	42.95	7.50	2.02
	Airfoil	MEL021				Airfoil	MEL031		
	Blade number Z	3				Blade number Z	2		
Runner B	Radius r [m]	0.019	0.095	0.171	Runner D	Radius r [m]	0.019	0.095	0.171
	Solidity	0.397	0.060	0.016		Solidity	0.394	0.070	0.016
	Blade angle θ [°]	42.95	7.50	2.02		Blade angle θ [°]	47.00	9.36	3.09
	Airfoil	MEL021				Airfoil	MEL031		
	Blade number Z	2				Blade number Z	2		

3. Method and Conditions for the Numerical Analysis

The general-purpose thermal fluid analysis code ANSYS CFX15.0 was used for the numerical analyses. In a composite body of this hydraulic turbine, the power coefficient is largely dependent on the interference between the runner and the diffuser section of an axially-asymmetrical collection device [11]. Therefore, three dimensional unsteady flow analysis for the composite body and three dimensional steady flow analysis for the single runner were performed. The governing equations are the conservation of mass equation [20] and the conservation of momentum equation [20]. The SST (Shear Stress Transport) model [21] was used for the turbulence model. Moreover, water was used for the working fluid.

For example, the computational model for Runner D composite body is shown in Figure 4, and the total computational region in Figure 5. Computational regions included a single runner or a composite body, their middle regions, and external regions. To assess the potential performance of the calculation object, we assumed that a uniform flow entered the extensive space (external region) in which the calculation object was placed [9-11]. Therefore, the influence of free surface and velocity distribution, etc. in the open channel is not considered. The external region is cylindrical with a diameter 10 times the outer diameter D of the runner. Moreover, the lengths upstream and downstream are 10 times and 15 times the length of the outer diameter D of the runner, respectively, and are measured from the center of the runner. Total calculation grids were composed of 2.57–2.92 and 3.33–3.67 million elements for the single runner and composite body analyses, respectively. We confirmed that the dependency on the number of grids was relatively small by increasing the total number of calculation grids by 1.5 times [10]. The boundary conditions were flow velocity v_∞ = 1.5 m/s for the inlet boundary, arbitrary rotational speed for the runner, and a static pressure (gauge pressure) of 0 Pa for the outlet boundary. The outer periphery of the external region was assigned as the slip condition and wall surfaces were assigned as the nonslip condition. The boundaries between the rotating and static systems were joined using the frozen rotor [22] technique in steady flow analyses, and the transient rotor–stator [22] technique in unsteady flow analyses. In steady flow analyses, the blade phase angle θ* was fixed to 0°.

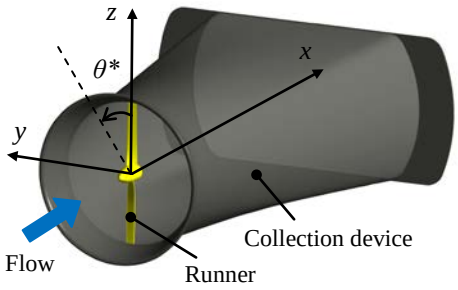

Fig. 4 Computational model (Runner D + C.D.)

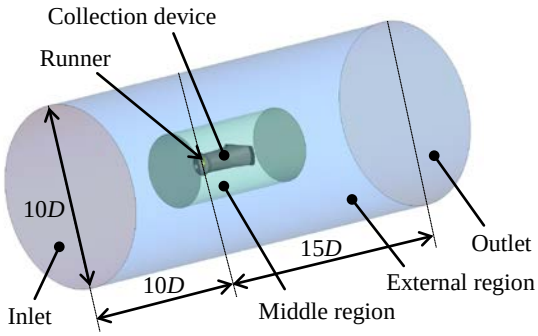

Fig. 5 Computational domain (Runner D + C.D.)

4. Results and Discussion

4.1 Comparison of Performance Characteristics

Figure 6 shows the correlation between the tip speed ratio λ and the power coefficient C_W of each single runner and the composite bodies. Here, the pressure and the wall shear stress acting on the blade surface were multiplied by the radius, and integrated to obtain the torque. Considering the single runners, the maximum values of C_W are 0.191 at λ = 5.0 for Runner A, 0.139 at λ = 5.0 for Runner B, 0.266 at λ = 5.7 for Runner C, and 0.265 at λ = 5.0 for Runner D; hence, Runner C has the largest value. The maximum values of C_W are greater in the case of three blades relative to two blades, and comparing within the two blade designs, the values are greater for MEL031 airfoil than for MEL021 airfoil. With respect to the composite bodies, the

maximum values of C_W are 0.573 at λ = 6.5 for Runner A, 0.645 at λ = 8.5 for Runner B, 0.623 at λ = 5.7 for Runner C, and 0.707 at λ = 5.7 for Runner D. The maximum values of C_W for Runners B, C, and D increased 1.13 times, 1.09 times, and 1.23 times, respectively, compared with the prototype Runner A.

Hence, we found that the composite body with two blades (MEL031 airfoil) with an altered blade angle had the largest values of C_W. In addition, the maximum values of C_W for Runners A, B, C, and D of the composite body increased by factors of 3.00, 4.64, 2.34, and 2.67, respectively, compared with the single runner. Therefore, the increase in the power coefficient because of the collection device became much larger with two blades of MEL021 airfoil.

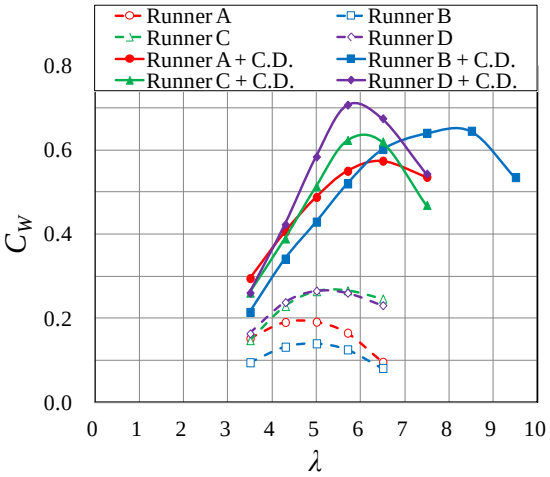

Fig. 6 Correlation between the tip speed ratio and the power coefficient

4.2 Comparison of Various Characteristics and the Flow Field

We examined the factors that increase the output by investigating the characteristics of each runner. The power coefficient C_W, the input power coefficient C_I and inlet velocity ratio K are obtained by the following equations [8],

$$C_W = \frac{W}{\rho A v_\infty^3 / 2} = \eta C_I \tag{1}$$

$$C_I = \frac{\left(\overline{P_1} - \overline{P_2}\right)Q}{\rho A v_\infty^3 / 2} = \psi K^3 \left(1 - \nu^2\right) \tag{2}$$

$$K = \frac{\overline{v_{a1}}}{v_\infty} = \sqrt{\frac{1 - C_{pb}}{1 - fC_{pd} + \psi}} \tag{3}$$

where C_{pd} is the diffuser pressure recovery coefficient, C_{pb} is the backpressure coefficient, f is the correction coefficient ($f \leqq 1$), η is the turbine efficiency, ν is the hub ratio, and ψ is the loading coefficient. The correction coefficient considers the change in performance of the collection device diffuser caused by the swirling flow at the outlet of the runner, the blade tip vortices, and the hub. It also considers the entrance loss of the collection device, which has been ignored thus far.

The loading coefficient ψ, inlet velocity ratio K, and input power coefficient C_I with reference to tip speed ratios λ of each runner and composite body are shown in Figs. 7, 8, and 9, respectively. In addition, the correlation between the loading coefficient and the input power coefficient or inlet velocity ratio is shown in Fig. 10. C_I and K in Fig. 10 were found theoretically from Eqs. (2) and (3) under the hypothesis of f = 1, using C_{pd} and C_{pb} obtained by the analysis of a single collection device.

From Fig. 7, it can be seen that ψ gradually increases with increasing λ for Runners A and B (for both single runners and composite bodies). In contrast, for Runners C and D, ψ significantly increases with increasing λ for both cases. In particular, in the case of composite bodies, ψ increases dramatically at $\lambda > 5.7$. As for Runner C, ψ became the largest (excluding the low tip speed ratio region) for both cases. Comparing Runners A and C, with respect to ψ of the composite bodies, Runner A showed higher values in the low-tip-speed-ratio region, whereas Runner C showed greater values in the high-tip-speed-ratio region. The value of λ where the reverse phenomenon of ψ occurs is in the vicinity of the tip speed ratio where the C_W of Runner C reaches the maximum. When C_W decreases for latter tip speed ratios, this may be influenced by the increase in ψ. This trend can also be verified with the static pressure distributions around the hydraulic turbine at λ = 6.5, as illustrated in Figures 11(a)–11(d). It can be seen that C_P in front of a runner is considerably larger for the Runner C composite body and slightly larger for the Runner D composite body, compared with that of Runner A.

From Fig. 8, it can be seen that Runner B has the largest inlet velocity ratio over the entire range of tip speed ratios for both the single runner and composite bodies, which is the opposite tendency relative to the loading coefficient. Runners C and D showed larger K values in the low-tip-speed-ratio region, but a smaller K in the high-tip-speed-ratio region, compared with Runner A. At λ = 6.5, K values for the composite bodies with Runners A–D increased 1.251 times, 1.470 times, 1.184 times, and 1.220 times, respectively, compared with each single runner. Accordingly, the runners of smaller loading coefficients have larger inlet velocity ratios and larger increases in inlet velocity ratios owing to the collection device.

As shown in Fig. 9, C_I values of Runner C for all the single runners were the largest throughout the entire range of tip speed ratios. Of all the composite bodies, C_I values of Runner B were the largest for the high tip speed ratios. The C_I values of Runners C and D sharply decreased at $\lambda > 5.7$. This point is in the vicinity of the tip speed ratio where the abovementioned ψ dramatically increased (the extreme increase in ψ reduced K). Runners C and D had large C_I values for low tip speed ratios. Specifically, the maximum value of C_I of Runner D is equivalent to that of Runner B. According to the theoretical values shown in Figure 10, this collection device showed the largest value of C_I at around ψ = 0.52. Therefore, the ψ of Runner D had a tendency to increase with the MEL031 blades. This is because the ψ value approaches that where the theoretical value of C_I reaches a maximum and thus the decrease of K occurs in the high tip speed ratios (when the number of blades was reduced to two with the altered blade angle). Hence, it is a useful and relatively simple method for adjusting the loading coefficient and increasing the input power coefficient by changing the number of blades.

The turbine efficiency η values for all cases studied are shown in Fig. 12. In addition, limiting streamlines on the suction surfaces of the blades are shown in Figs. 13–16. Here, L.E. refers to the leading edge and T.E. to the trailing edge. As shown in Fig. 12, the maximum values of η for the runners of composite bodies shift to the higher-tip-speed-ratio side compared with those for the single runners similarly to the C_W data. As for Runners A and B, the maximum values of η for the composite bodies tended to slightly increase relative to those for the single runners. In contrast, for Runners C and D, the maximum values of η for the composite bodies tended to slightly decrease relative to the case of single runners. Comparing the maximum η of Runners A and B, the former showed a larger value for single runners, whereas the latter had a larger value for the composite bodies. Runner C (MEL031) always showed a maximum value of η larger than that of Runner B, whereas Runner D for which the blade angle was altered had the largest value overall when.

In reference to Figures 13–16, although at λ = 6.5, the Runner A composite body at had a separation from the hub point to midpoint, it maintained a relatively good flow state from the midpoint to tip. In contrast, the Runner B composite body showed a major separation from the hub point to close to the tip because the attack angle became excessively large with increasing K. This separation area became slightly smaller at λ = 7.5, which represents the maximum efficiency of the Runner B composite body. Conversely, at λ = 6.5, the Runner C composite body had almost the same area of separation as the Runner A composite body. Thus, the reason the maximum efficiency of the Runner C composite body is higher than that of Runner A composite body, even though the separation areas of both composite bodies are almost the same, appears to be because the drag-lift ratio of MEL031 in the vicinity of the low Reynolds number (1×10^5) is lower than that of MEL021. In addition, the separation area of the Runner D composite body is reduced compared with that of Runner C, which appears to contribute to the high efficiency of the Runner D composite body.

The maximum values of the input power coefficient of the composite bodies with two MEL031 blades and altered blade angle are equivalent to those of the composite bodies with two MEL021 blades. Hence, we can conclude that the composite bodies with two MEL031 blades and altered blade angle had the highest turbine efficiency and as a result the largest power coefficient.

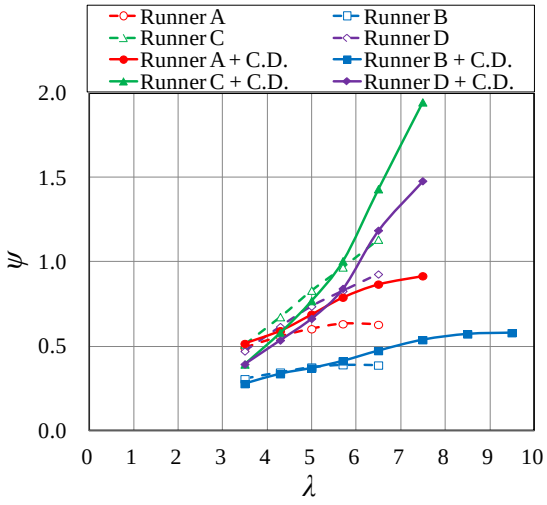

Fig. 7 Correlation between the tip speed ratio and the loading coefficient

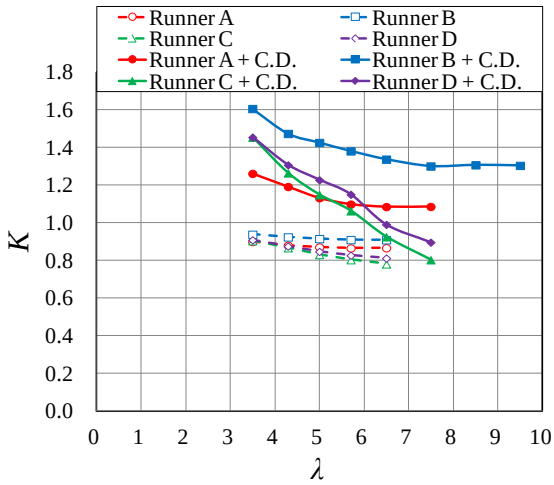

Fig. 8 Correlation between the tip speed ratio and the inlet velocity ratio

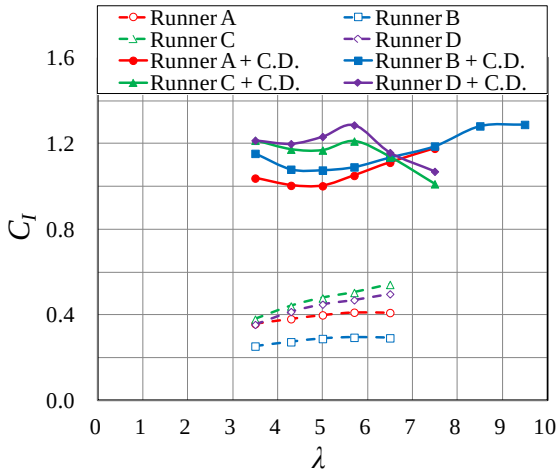

Fig. 9 Correlation between the tip speed ratio and the input power coefficient

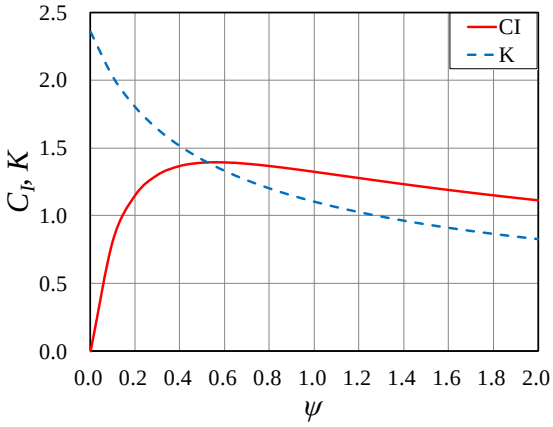

Fig. 10 Effect of the loading coefficient on the input power coefficient and inlet velocity ratio

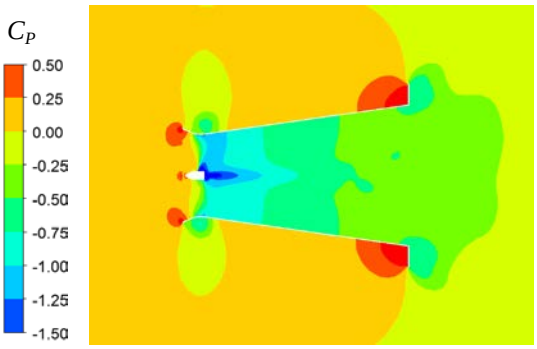

(a) Runner A + C.D.

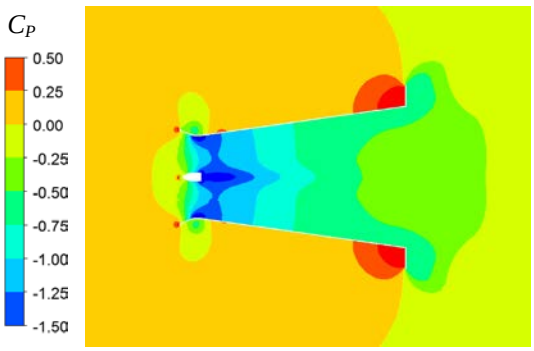

(b) Runner B + C.D.

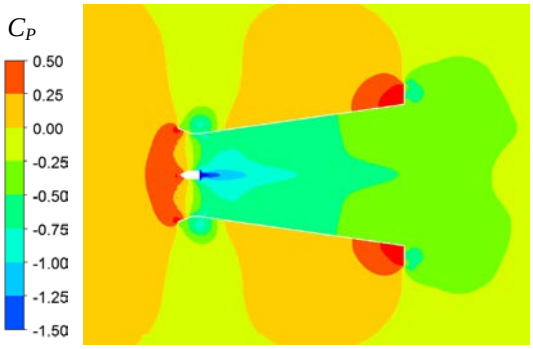

(c) Runner C + C.D.

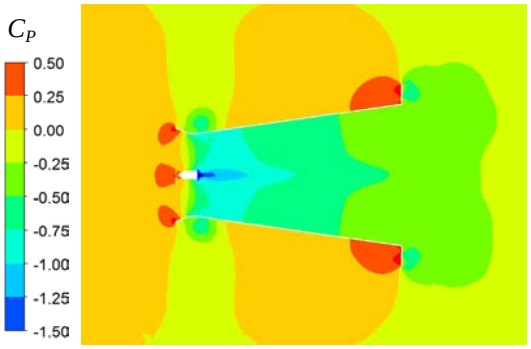

(d) Runner D + C.D.

Fig. 11 Static pressure distributions at λ = 6.5 (x-y section, θ^* = 0)

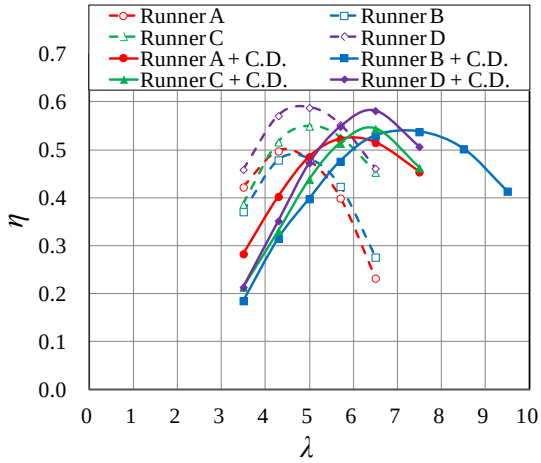

Fig. 12 Correlation between the tip speed ratio and the turbine efficiency

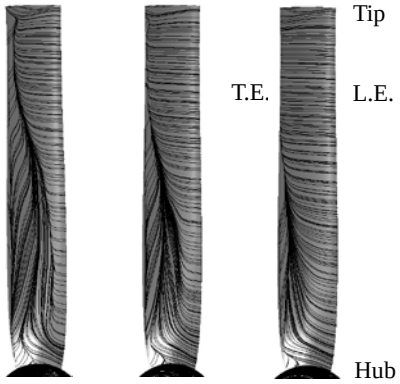

(a) λ=5.7 (b) λ=6.5 (c) λ=7.5

Fig. 13 Limiting stream line on suction surface (Runner A + C.D.)

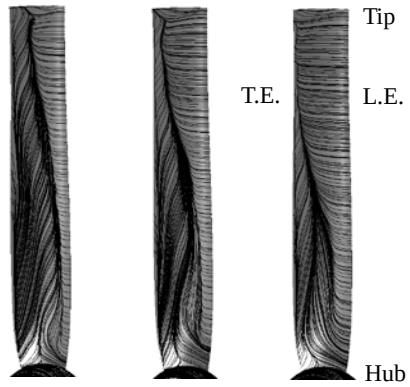

(a) λ=5.7 (b) λ=6.5 (c) λ=7.5

Fig. 14 Limiting stream line on suction surface (Runner B + C.D.)

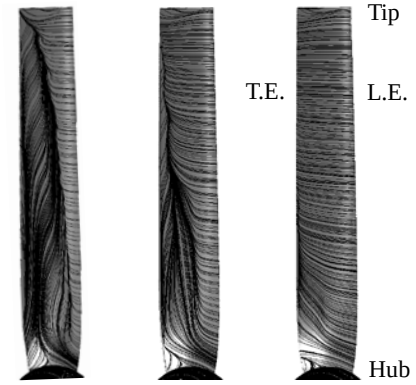

(a) λ=5.7 (b) λ=6.5 (c) λ=7.5

Fig. 15 Limiting stream line on suction surface (Runner C + C.D.)

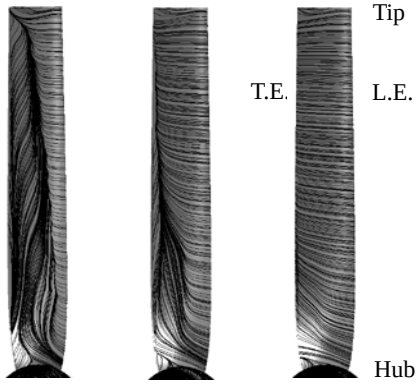

(a) λ=5.7 (b) λ=6.5 (c) λ=7.5

Fig. 16 Limiting stream line on suction surface (Runner D + C.D.)

4.3 Experimental Verification

To verify the results of the numerical analysis of the hydraulic turbine, we performed a test in the canal in Tadamimachi in the Minamiaizu District of Fukushima prefecture [10]. For example, the prototype for Runner D composite body used in the verification test is shown in Figures 17. The prototype comprised the runner, the collection device and the generator. Two runners, A and D, were used. The specifications of two kinds of runners and collection device are generally the same as those previously described for the computational model. The waterway width of the open channel was about 1900 mm and the water depth was about 570 mm. The flow velocity of the open channel was measured with a propeller meter at 380 mm upstream of the hydraulic turbine, before the hydraulic turbine was placed. The average flow velocity calculated by a two-point method was 1.72 m/s.

The actual value for the output power W obtained from the verification test is shown in Figure 18. It is shown together with the value of W calculated from C_W of the composite body for v_∞ = 1.72 m/s. However, the measured value of W is the value found by adding the actual inverter loss, power transmission loss, and generator loss, which are all measured beforehand, to the inverter output power. As can be seen from Fig. 18, the measured values are consistent with the calculations in terms of the tendency where the W of the Runner D composite body is larger than that of the Runner A composite body. The difference between the measurement and calculated values appears to be because the average flow velocity of the open-channel flow cannot be measured with high precision in the verification test. Moreover, it appears to be because the influence of the free surface and velocity distribution for the open-channel flow, and the form of the power transmission device are not taken into consideration in the numerical analysis. The maximum measured values of Runner A and Runner D composite bodies are 156.4 W at n = 496 min^{-1} and 200.5 W at n = 583 min^{-1}, respectively. Accordingly, the maximum W value of the Runner D composite body was about 1.28 times larger than that of Runner A.

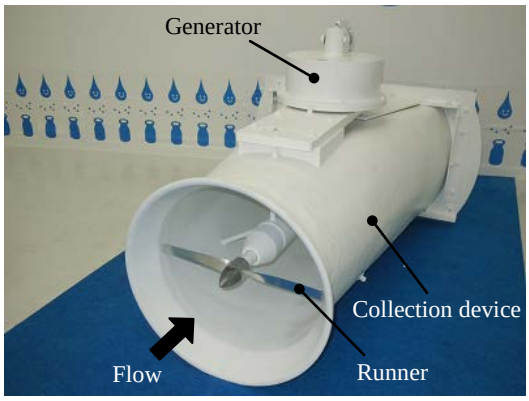

Fig. 17 Prototype model (Runner D + C.D.)

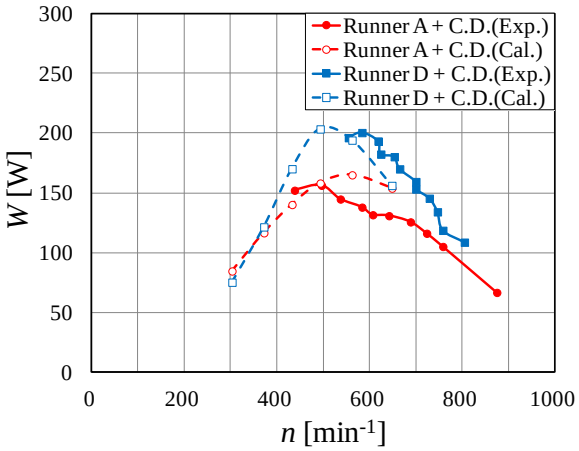

Fig. 18 Correlation between the rotational speed and the output power

5. Conclusions

In this study, with the aim to improving the performance of axial flow hydraulic turbine with a collection device, we examined through numerical analysis the performance and flow field of various single runners and composite bodies of runners with collection devices, where the airfoil and number of blades was also varied.

(1) In the case of a single runner, the maximum power coefficient was larger for three blades than two blades and for MEL031 airfoil compared with MEL021 airfoil.

(2) The maximum values of input power coefficient of the Runner D composite body with two blades (which adopts the MEL031 airfoil and alters the blade angle) are equivalent to those of the composite body with two blades (MEL021 airfoil). We found that the Runner D composite body has the highest turbine efficiency and thus the largest power coefficient.

(3) For the two blade runners with MEL031 airfoil, the input power coefficient increased for single runners, but rapidly decreases for composite bodies at the high-tip-speed-ratio region. This is because the loading coefficient rapidly increased at the high-tip-speed-ratio region; hence, the inlet velocity ratio decreased.

(4) In a verification test using an open-channel water flow with an average flow speed of 1.72 m/s and water depth of 530 mm, the maximum output power of the Runner D composite body was 200.5 W at n = 583 min^{-1}, which was 1.28 times higher than that of the Runner A composite body.

We acknowledge that a part of the study has been subsidized by Program for Revitalization Promotion, JST (Potential Test Type α). We express our gratitude here.

Nomenclature

A	Water-receiving area [m^2] $=\pi r_t^2$	r	Runner radius [m]
C_I	Input power coefficient $=\left(\overline{P_1}-\overline{P_2}\right)Q/\left(\rho A v_\infty^3/2\right)$	v	Absolute velocity [m/s]
C_P	Pressure coefficient $=\left(P-P_\infty\right)/\left(\rho v_\infty^2/2\right)$	W	Output power [W]
C_{pb}	Backpressure coefficient $=\left(\overline{P_3}-P_\infty\right)/\left(\rho v_\infty^2/2\right)$	η	Turbine efficiency $=C_W/C_I$
C_{pd}	Diffuser pressure recovery coefficient $=\left(\overline{P_3}-\overline{P_2}\right)/\left(\rho \overline{v_{a1}}^2/2\right)$	θ	Blade angle [°]
		θ*	Blade phase angle [°]
C_W	Power coefficient $=W/\left(\rho A v_\infty^3/2\right)$	λ	Tip speed ratio $=r_t\omega/v_\infty$
f	Correction coefficient	ν	Hub ratio $=r_h/r_t$
K	Inlet velocity ratio $=\overline{v_{a1}}/v_\infty$	ρ	Fluid density [kg/m^3]
n	Rotational speed [min^{-1}]	ψ	Loading coefficient $=\left(\overline{P_1}-\overline{P_2}\right)/\left(\rho \overline{v_{a1}}^2/2\right)$
P	Static pressure (gauge pressure) [Pa]	ω	Rotational angular velocity [rad/s]
Q	Flow rate through the runner [m^3/s] $=A\overline{v_{a1}}$		

Subscripts

1	Just before the runner	h	Hub
2	Just after the runner	t	Tip
3	Collection device outlet	∞	Infinite distance
a	Axial component	—	Average value for the flow rate

References

[1] C. Nicolet, A. Zobeiri, P. Maruzewski, F. Avellan, 2011, “Experimental Investigations on Upper Part Load Vortex Rope Pressure Fluctuations in Francis Turbine Draft Tube,” International Journal of Fluid Machinery and Systems, Vol. 4, No. 1, pp. 179-190.

[2] T. S. Reynolds, 1983, “Stronger Than A Hundred Men: A History of the Vertical Water Wheel,” The Johns Hopkins University Press.

[3] Y. Fujiwara, H. Kado and Y. Hosokawa, 1987, “History and Performance of Traditional Water wheel in Western Europe,” Transactions of the Japan Society of Mechanical Engineers, Vol. 90, No. 819, pp. 212-218. (in Japanese)

[4] D. Capecchi, 2013, “Over and Undershot Waterwheels in the 18th Century. Science-Technology Controversy,” Advances in Historical Studies, Vol. 2, No. 3, pp. 131-139.

[5] M. Anyi and B. Kirke, 2010, “Evaluation of small axial flow hydrokinetic turbines for remote communities,” Energy for Sustainable Development, Vol. 14, pp. 110-116.

[6] A. Inagaki and T. Kanemoto, 2005, “Performance of Gyro-Type Hydraulic Turbine Suitable for Shallow Stream,” Turbomachinery, Vol. 33, No. 10, pp. 614-621. (in Japanese)

[7] M. Nakajima, S. Iio and T. Ikeda, 2008, “Performance of Savonius Rotor for Environmentally Friendly Hydraulic Turbine,” Journal of Fluid Science and Technology, Vol. 3, No. 3, pp. 420-429.

[8] M. Inoue, A. Sakurai and Y. Ohya, 2002, “A Simple Theory of Wind Turibine with Brimmed Diffuser,” Turbomachinery, Vol. 30, No. 8, pp. 497-502. (in Japanese)

[9] Y. Nishi, T. Inagaki, K. Okubo and N. Kikuchi, 2013, “Study on the Development of an Axial Flow Hydraulic Turbine with a Collection Device,” Turbomachinery, Vol. 41, No. 4, pp. 233-241. (in Japanese)

[10] Y. Nishi, T. Inagaki, K. Okubo and N. Kikuchi, 2014, “Study on an Axial Flow Hydraulic Turbine with Collection Device,” International Journal of Rotating Machinery, Vol. 2014 Article ID 308058, pp. 1-11.

[11] Y. Nishi, T. Inagaki, Yanrong Li, Sou Hirama and N. Kikuchi, 2015, “Unsteady Flow Analysis of an Axial Flow Hydraulic Turbine with Collection Devices Comprising a Different Number of Blades,” Journal of Thermal Science, Vol. 24, No. 3, pp. 239-245.

[12] Y. Ohya, T. Karasudani and A. Sakurai, 2002, “Development of High-Performance Wind Turbine with Brimmed Diffuser,” Journal of the Japan Society for Aeronautical and Space Sciences, Vol. 50, No. 587, pp. 477-482. (in Japanese)

[13] K. Toshimitsu, K. Nishikawa, W. Haruki, S. Oono, M. Takao and Y. Ohya, 2008, “PIV Measurements of Flows around the Wind Turbines with a Flanged-Diffuser Shroud,” Journal of Thermal Science, Vol. 17, No. 4, pp. 375-380.

[14] Y. Ohya and T. Karasudani, 2010, “A Shrouded Wind Turbine Generating High Output Power with Wind-lens Technology,” Energies, Vol. 3, pp. 634-649.

[15] M. J. Khan, G. Bhuyan, M. T. Iqbal and J. E. Quaicoe, 2009, “Hydrokinetic energy conversion systems and assessment of horizontal and vertical axis turbines for river and tidal applications: A technology status review,” Applied Energy, Vol. 86, pp. 1823-1835.

[16] David L. F. Gaden and Eric L. Bibeau, 2010, “A numerical investigation into the effect of diffusers on the performance of hydro kinetic turbines using a validated momentum source turbine model,” Renewable Energy, Vol. 35, pp. 1152-1158.

[17] B. Cui, Z. Song, Y. Zhang, Y. Jin and Y. Lin, 2012, “Influence of Additional Device on Performance of the Marine Current Turbine,” Open Journal of Fluid Dynamics, Vol. 2, pp. 305-310.

[18] H. Sun and Y. Kyozuka, 2012, “Experimental Validation and Numerical Simulation Evaluation of a Shrouded Tidal Current Turbine,” Journal of the Japan Society of Naval Architects and Ocean Engineers, Vol. 16, pp. 25-32.

[19] H. Matsumiya, T. Kogaki, M. Iida and K. Kieda, 2001, “Development of a high performance airfoil,” Turbomachinery, Vol. 29, No. 9, pp. 519-524. (in Japanese)

[20] ANSYS, Inc., 2010, “ANSYS CFX-Solver Theoretical guide,” pp. 22-23. (in Japanese)

[21] ANSYS, Inc., 2010, “ANSYS CFX-Solver Theoretical guide,” pp. 81-85. (in Japanese)

[22] ANSYS, Inc., 2010, “ANSYS CFX-Solver Modeling guide,” pp. 142-145. (in Japanese)